

# Probing Molecular Solids with Low-Energy Ions

Soumabha Bag, Radha Gobinda Bhui,  
Ganapati Natarajan, and T. Pradeep

DST Unit of Nanoscience, Department of Chemistry, Indian Institute of Technology Madras, Chennai 600036, India; email: pradeep@iitm.ac.in

Annu. Rev. Anal. Chem. 2013. 6:97–118

First published online as a Review in Advance on March 14, 2013

The *Annual Review of Analytical Chemistry* is online at [anchem.annualreviews.org](http://anchem.annualreviews.org)

This article's doi:  
10.1146/annurev-anchem-062012-092547

Copyright © 2013 by Annual Reviews.  
All rights reserved

## Keywords

ice, mass spectrometry, soft landing, ion scattering, self-assembled monolayers, phase transition

## Abstract

Ion/surface collisions in the ultralow- to low-energy (1–100-eV) window represent an excellent technique for investigation of the properties of condensed molecular solids at low temperatures. For example, this technique has revealed the unique physical and chemical processes that occur on the surface of ice, versus the liquid and vapor phases of water. Such instrument-dependent research, which is usually performed with spectroscopy and mass spectrometry, has led to new directions in studies of molecular materials. In this review, we discuss some interesting results and highlight recent developments in the area. We hope that access to the study of molecular solids with extreme surface specificity, as described here, will encourage investigators to explore new areas of research, some of which are outlined in this review.

## 1. INTRODUCTION

Chemical phenomena in molecular solids have implications for physics, materials science, biology, and industry. These diverse processes range from adsorption, catalysis, wetting, and diffusion to molecular recognition and self-organization—all of which are central to chemical and biological functionality. Elementary steps involved in these molecular events can lead to complex overall phenomena and require detailed studies of well-characterized surfaces under precise conditions. Mass-selected ions of known kinetic energy impinging on ultrathin films of molecules represent an excellent system in which various chemical phenomena can be modeled. This review outlines some of the most fascinating recent advances in this developing and instrumentation-intensive area.

Molecular solids are composed of periodically arranged molecules that form a lattice. This periodicity may be short or long range, as in amorphous or crystalline solids, respectively. Such solids are not common in the natural environment, where extended solids, such as silica, dominate. The most common molecular solid is water ice; phenomena that occur on the surface of this solid play pivotal roles in atmospheric chemistry, as in the case of ozone layer depletion (1–3). Although elementary chemical reactions such as chlorine radical formation and reactions have been studied, issues such as molecular diffusion, cage formation, and reactivity are important for molecular solids under different pressure and temperature conditions, as in the case of gas hydrates. Thus, molecular chemistry spans a wide range of thermodynamic conditions, from ice particles in interstellar space at  $10^{-15}$  bar to gas-hydrate formation at  $10^5$  bar; this review is limited to low-pressure conditions. At low pressure, the molecular flux is correspondingly small, so investigations can be performed only in ultrasensitive environments.

**Figure 1** depicts hexagonal crystalline ice (Ih) grown on a Ru(0001) substrate; specifically, three layers of ruthenium atoms in a hexagonal arrangement are shown. During epitaxial growth on the ruthenium surface, the first layer of water molecules is adsorbed onto the surface. A second layer then develops; it is connected by hydrogen bonds to the first layer of water molecules to form a hexagonal cage-like arrangement. In this geometry, each alternative molecule is situated equidistantly above or below a central plane to form a tetrahedral environment. Together, these two layers are known as a bilayer (4). The second layer of water molecules is considered half of the bilayer (hence the term half-bilayer) (**Figure 1**). The bilayer reproduces itself with an interlayer distance of 2.75 Å (5) to produce an Ih network. In **Figure 1**, the atoms are projected toward the reader, away from the text; therefore, the nearest atoms appear largest. Because of this effect, the first and second bilayers appear to have different thicknesses. Because water molecules orient epitaxially on the ruthenium surface, Ru(0001) is an ideal substrate for ice film growth. However, the orientation of water molecules at the ruthenium–ice interface is uncertain.

Typically, all such experiments are performed in ultrahigh-vacuum (UHV) conditions at around  $10^{-10}$  torr. Water vapor is usually condensed on a cold metal surface, typically single crystals whose solid-state structure is similar to that of crystalline ice (CW), to generate thin ice films. The growth of an ice film and its structure are sensitive to the metal surface. Density functional theory calculations suggest that the metal–water interaction is very strong in the case of Ru(0001) surfaces (6). On a Ru(0001) surface, ice growth begins with a small cluster (7). Three-dimensional film growth then occurs through the reproduction of bilayers (7), as described above. In practice, amorphous ice (ASW) is prepared through the deposition of water vapor below 120 K (8). Thereafter, annealing at a temperature above 140 K generates CW. High-density ASW or compact ASW, which has very low porosity, can be prepared by growth of the ice film at  $\sim 125$  K (9). However, the temperature depends on parameters such as the nature of the surface, the rate of deposition, the annealing rate, and time (5).

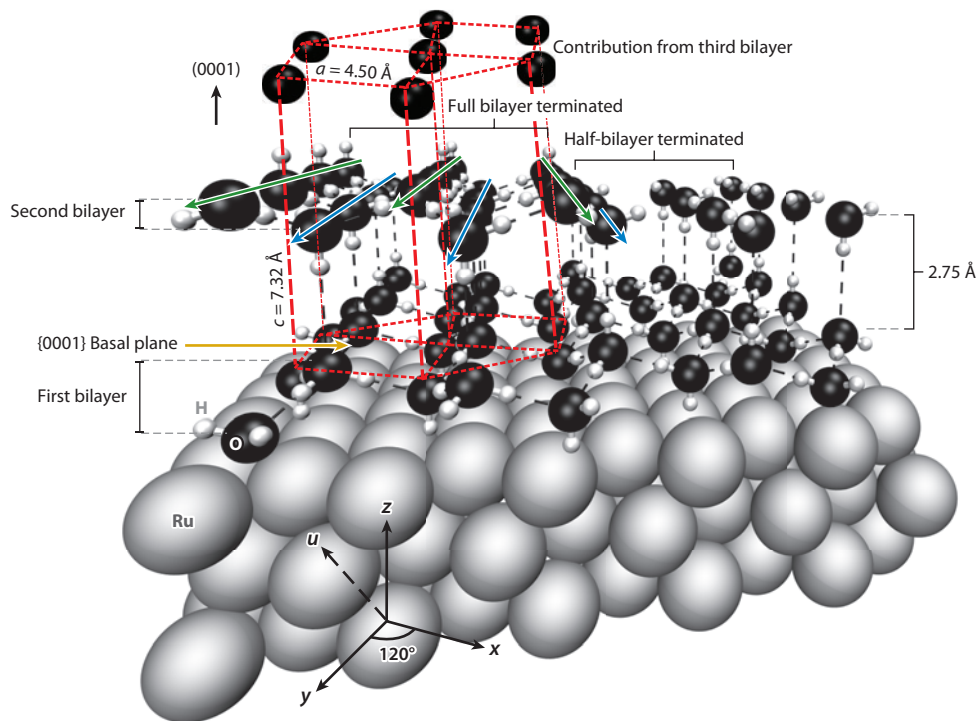


**Figure 1**

Hexagonal ice growth on a Ru(0001) substrate. The gray balls represent ruthenium atoms, the black balls represent oxygen atoms, and the white balls represent hydrogen atoms. Hydrogen bonds in the ice structure are indicated by the black dashed line between the water molecules. The epitaxial growth of the ice is also depicted. After the ice layer is extended to another bilayer, a unit cell of hexagonal ice can grow. For clarity, the central plane, composed of the second bilayer, is not shown. The circles on the top {0001} plane of the unit cell represent the oxygen atoms forming the third bilayer. The basal {0001} plane is marked by a yellow arrow. Red dashed lines show the unit cell of ice. In the unit cell,  $a$  and  $c$  stand for lattice constants of hexagonal ice;  $a$  is 4.50 Å, and  $c$  is 7.32 Å. The water molecules forming two half-bilayers (making the full bilayer) are indicated by blue and green arrows. The water molecules arranged along the blue arrow, if extended to the right, form a half-bilayer. This figure is based on several inputs from the literature.

Several techniques have been used to investigate the crystal structure of adsorbed ice films. Of these, helium diffraction and low-energy electron diffraction (LEED) are discussed here. Use of these techniques showed that an ice(0001) film grown on Ru(0001), Pt(111), or Pd(111) terminates as a full bilayer rather than as a half-bilayer (5, 10–12). However, LEED  $I$ - $V$  (intensity–voltage) experiments (10) and total energy calculations (13) revealed that the topmost layer of the film is modified significantly (5). Also, the upper monolayers undergo large-amplitude vibrational motions, such that the oxygen atoms become invisible to LEED (5, 12). The small ( $2 \times 2$ ) peak in helium diffraction experiments suggests that the topmost layer undergoes reconstruction (12). X-ray absorption studies of the intermolecular distance between ice layers indicated that the interlayer distance at the surface is greater than that in bulk (5).

In addition to the aforementioned techniques, a common analytical method used to study adsorbed molecules is temperature-programmed desorption (TPD) (14–17). Desorption of molecules from ice surfaces can be accompanied by processes in the surface that include diffusion

(18–21), molecular volcano (19), crystallization (22, 23), and polymerization events, all of which have been the subjects of detailed studies. We can better understand the molecular details of processes taking place in such solids by using vibrational spectroscopy, which in conjunction with TPD is often an indispensable tool (24–45). Also, surface-sensitive tools, such as X-ray photoelectron spectroscopy (XPS), have been employed with TPD to study ice films (26, 46). Ions whose energy ranges between 1 and 100 eV (47–71)—which is known as the hyperthermal energy regime and, especially with energies below 10 eV (9, 72, 73), constitutes the ultralow-energy regime—are novel probes for studies of new phenomena. Their novelty arises from the extremely short interaction time between the ions and the surface. For example, Cs<sup>+</sup> ions impinging on a surface with 50-eV translational energy are present only for a few tens of femtoseconds in the vicinity of 10 to 20 monolayers (measured typically in terms of exposure in Langmuirs; 1 Langmuir =  $1 \times 10^{-6}$  torr s of exposure) of condensed molecular solids. The term vicinity refers to an area of radius 4 Å in which chemical interactions can occur (74). First, this extremely short interaction time allows the ions to “observe” the dynamic events of the surface at ultrashort timescales. Second, assuming 10–15% translational-vibrational energy transfer efficiency (74) in collisional events, the surface is sufficiently excited to undergo change in itself or to cause modifications to the colliding ions. This phenomenon causes either reactions or accommodation of the products of collision that preserves the chemical nature of the partners and is known as soft landing (75). Third, given that the collision event is precisely controlled, chemical modifications can be made systematically. Fourth, because the ion beam can be controlled in time, as in the case of an ion pulse, the dynamics of the events can be sampled. Fifth, because the ions possess mass, energy, and direction, all these parameters can be individually or jointly used to capture information on events occurring at the surface. Although many of these low-energy ion phenomena have not yet been investigated adequately, future explorations will undoubtedly be rewarding.

The microscopic processes that occur in these interactions strongly depend on the nature of the projectile, its collision partner on the surface, its geometry and orientation, and the energy of impact. Depending on all these parameters, various techniques (**Table 1**) have been employed to study ion scattering processes. Certain factors, such as (*a*) the ability to create surfaces of interest and manipulate ions with distinct energy, (*b*) the capacity to perform reactions with species derived from mass-selected ions, and (*c*) the ability to carry out reactions in controlled conditions, have contributed to the development of these techniques. All of these processes can broadly be referred to as low-energy ion scattering (LEIS). Therefore, we use this acronym to describe the diverse phenomena that occur in this energy window.

Below, we briefly discuss the instrumentation used to study low-energy ion impact phenomena in molecular solids. We then provide an account of fascinating recent results and describe highlights from the current literature. Finally, we conclude with future directions.

## 2. INSTRUMENTATION

As mentioned above, this area of research depends greatly on appropriate instrumentation. In this section, we discuss several important techniques.

The essential purpose of instrumentation is evident from the title of this review. Instruments enable production of low-energy ions, impact of ions at molecular surfaces, and analysis of the products and their properties. Depending on the details of the investigation being performed, additional components may be added. The primary instrument may be coupled with other techniques to probe surfaces and ions in more detail. In their simplest configuration, the instrumentation should be capable of ion production and product ion analysis.

**Table 1** Various low-energy ion scattering processes

Technique	Abbreviation	Energy range	Use	References
Reactive ion scattering	RIS	10–25 eV	Detection of ionic and neutral species from the surface following ion collisions	76–78
Low-energy sputtering	LES	30–100 eV	Detection of preexisting surface ions at the topmost layer by ion impact	76–78
Reactive landing	RL	10–20 eV	Surface reaction and patterning of molecules on active surfaces by ion impact	79–81
Soft landing	SL	10–20 eV	Deposition of polyatomic ions without damage at the surface by ion collisions	75, 82
Surface-induced dissociation	SID	20–200 eV	Fragmentation of projectile ions and associated chemical reactions	65, 74
Ion/surface reactions	I/S reactions	20–100 eV	Chemical reactions between impinging ions at molecular solids or monolayers	65, 83–85
Chemical sputtering	CS	30–350 eV	Ejection of surface species as ions after charge transfer from the projectile	5, 74, 86

The simplest instruments have two stages. In the first stage, an ion of interest, produced by an ion source, is energy-selected by an analyzer and subsequently collided with a molecular solid surface. In the second stage, the scattered or product ions arising from the surfaces are analyzed by a mass and/or energy analyzer. In addition to mass spectrometry, other techniques that can probe molecular solids are reflection absorption IR spectroscopy (RAIRS), TPD, and XPS. **Figure 2** depicts a typical LEIS instrument coupled with associated components. We briefly describe some of these components below.

## 2.1. Vacuum System

All ion scattering/collision experiments are carried out under UHV conditions (pressure  $<10^{-10}$  mbar) to obtain clean surfaces and to avoid loss of ions due to interactions with gas-phase molecules. Vacuum chambers are made of stainless steel and are connected with a vacuum system to achieve optimum pressure. A vacuum system generally contains turbo molecular pumps (TMPs) backed by additional TMPs and connected to displacement pumps, such as rotary vane or diaphragm pumps. Diaphragm pumps, although more expensive than rotary vane pumps, do not release hydrocarbons. Entrapment pumps, such as titanium sublimation pumps or cryopumps, can be used to create a high vacuum.

## 2.2. Ion Source

In ion scattering experiments, it is necessary to produce projectile ions prior to collision. Ionization methods depend mainly on two factors, namely the ion of interest and the design of the instrument.

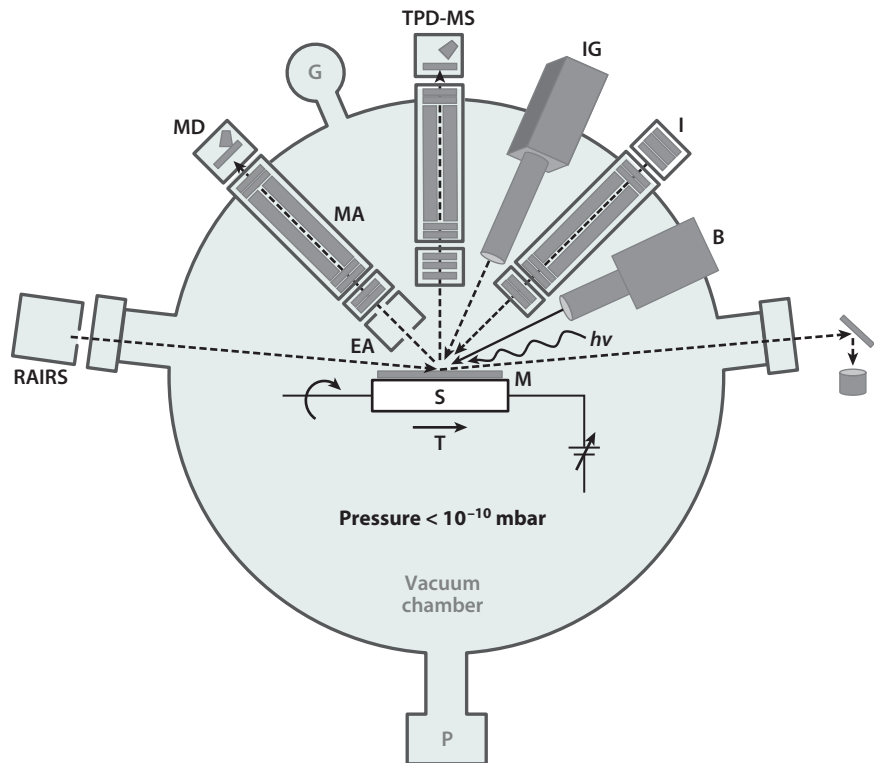


**Figure 2**

Typical low-energy ion scattering instrument. The circle represents the vacuum chamber connected to the vacuum pump and the pressure gauge. A rotatable substrate is placed at the center of the vacuum chamber, onto which several molecular solids can be deposited. The temperature of the substrate can be regulated by the combined use of a cryostat and a heater. The substrate is connected to a potentiometer, through which voltage to the substrate can be applied. Also shown is a molecular beam deposition module (B), which generates a molecular solid film at slow deposition rates to allow epitaxial growth of the molecules at low temperatures. Abbreviations: EA, energy analyzer; G, pressure gauge;  $h\nu$ , light source; I, ion source; IG, ion gun; M, molecular solid; MA, mass analyzer; MD, mass detector; P, vacuum pump; RAIRS, reflection absorption IR spectrometer; S, substrate; TPD-MS, temperature-programmed desorption–mass spectrometer.

The most common ionization methods used in ion/surface collision are electron impact ionization, chemical ionization, and laser-induced ionization. Among these techniques, electron impact ionization is the most common because of the stability of the ion current and the small spread of the ions' kinetic energy. Recently, electrospray ionization and laser desorption/ionization methods were used to produce more complex ions that cannot be created with conventional methods. Several other ion sources (for instance, thermal ionization that produces  $\text{Cs}^+$  and  $\text{Li}^+$  ions) are also available.

### 2.3. Mass Spectrometers

The ions are mass-selected and collided on the surface, and the scattered ions are then analyzed with mass spectrometric techniques. Various mass analyzers, such as time-of-flight (TOF), magnetic

sector, quadrupole, linear quadrupole ion trap (56), quadrupole ion trap, Fourier transform–ion cyclotron resonance (FT-ICR), and orbitrap analyzers, may be used for this purpose; we describe the main types in this section.

In a TOF analyzer, ions with different mass-to-charge ratios are dispersed in time after flight through a field-free drift path of known length. The advantages of TOF include the ability to detect high mass ions and efficient analysis of product ions. Magnetic sector analyzers are momentum analyzers; the charged particles are separated by momentum-to-charge ratio in a magnetic field due to the Lorentz force. Quadrupoles are widely used mass analyzers that provide excellent ion transmission and mass resolution. At least three instruments, located at the Indian Institute of Technology (IIT) Madras (52, 53), the Israel Institute of Technology (87), and the University of Arizona (88), use a quadrupole as the mass analyzer in both ion selection and analysis chambers. The instrumental designs used at IIT Madras and Arizona are very similar: Two quadrupoles are positioned at 90°, and at the intersection of the ion optics is a surface whose collision angle is 45° with respect to the surface normal.

FT-ICR mass spectrometers offer very high resolving power and the highest available mass accuracy. One can study the energy of the scattered ions ejected from the surface after projectile ion collision prior to mass analysis by placing an energy analyzer immediately before the mass analyzer. Such analyses can also be performed by stopping potential measurements in quadrupole instruments.

## 2.4. Temperature-Programmed Desorption

TPD is a widely used spectroscopic technique in which gaseous molecules or atoms adsorbed onto a surface are analyzed by desorption during heating. Heating is carried out by linear temperature ramps. In TPD, the desorbed particles are analyzed either by a pressure gauge or by a mass spectrometer. TPD provides information about, for example, the heat of adsorption, adsorbate coverage, dissociative and nondissociative adsorption processes, the kinetics of desorption, the type of adsorption sites, surface reactions, and the entropy of desorption.

## 2.5. Reflection Absorption IR Spectroscopy

RAIRS is a well-known surface-sensitive spectroscopic method. In this technique, the incident IR beam (polarized or otherwise) is measured in absorption mode with an external detector following reflection from the surface under study (Figure 2). Through measurements of specific vibrational features, RAIRS provides information about the nature of the surface species that arise from surface reactions. It is a powerful tool for surface structure determination due to the dependence of absorption on the polarization of light. RAIRS is an important tool for determination of the binding site of adsorbates such as CO and NO, and it supplies information about the surface reaction pathways for catalytic processes.

# 3. RESULTS

## 3.1. Studies Using Self-Assembled Monolayers

One of the most-studied types of molecular solids consists of self-assembled monolayers (SAMs), which are highly ordered molecular films grown on a well-defined surface, usually Au(111). To provide a glimpse into the diverse phenomena that can be observed through LEIS, we present the surprising finding of multiple fluorine abstraction by a single  $W^+$  ion collision event on a

fluorinated SAM.  $W^+$  ions with a laboratory collision energy of 30 eV, produced from the impact of  $W(CO)_6$  molecules on a  $CF_3$ -terminated SAM (F-SAM) grown on Au(111), to provide a set of peaks corresponding to  $WF_n^+$  ions ( $n = 1, 2, \dots, 5$ ) with a unique intensity pattern (89). Such transition-metal chemistry was subsequently extended to many ions and surfaces in an effort to better understand the chemical nature of surfaces with extreme surface sensitivity. The projectile ions used in these so-called pickup reactions can be considered as chemical probes and used to understand the surface. However, this process also can cause surface transformations that can be used to pattern surfaces with reaction products formed by fluorine removal at selected impact sites. A fascinating aspect of these collisions is the relative interaction between such F-SAM surfaces and certain ions. Miller et al. (82) exploited this property to develop nonreactive patterning based on ion soft landing. Developments in this area have been described in detail elsewhere (81, 90).

Another widely studied molecular solid is water ice. The properties, surface structure, and reactions of ice have been studied in significant detail because of their importance to several chemical and physical processes that occur at low temperatures (90, 91), as well as their catalytic role in polar stratospheric clouds in the depletion of the ozone layer (1–3, 92) and their relevance in chemistry in the interstellar medium (25, 93–95). Ice surfaces prepared at low temperatures offer a unique environment in which to investigate various chemical and physical processes, such as diffusion (21), cluster formation (40, 41), phase transition (96, 97), chemical reaction, hydrogen/deuterium exchange (98–106), interactions with small molecules (46), and adsorption (26, 30). All these phenomena can be promoted and/or identified with hyperthermal energy (1–100-eV) ion collisions. They can also be followed with other well-known detection techniques. Several reviews on this topic are available (48, 74, 81, 86, 107–109). Below, we describe some of these studies to illustrate recent developments.

### 3.2. Molecular Diffusion/Intermixing

Hyperthermal energy ion collision is an effective technique for the study of ice surfaces and diffusion processes within an ice structure. At low temperatures, ice surfaces provide a reaction environment that is unique in comparison with that of the liquid state. Diffusional mixing of  $H_2O$  and  $D_2O$  has been investigated with LEIS (110). In this study, the authors deposited amorphous  $H_2O$  onto a ruthenium substrate and performed fractional deposition of  $D_2O$  onto the  $H_2O$  surfaces in the temperature range between 100 and 140 K, followed by time-dependent reactive ion scattering. The time required for interlayer mixing was approximately 1 h at 100 K, but at 140 K, it was several seconds. At higher temperatures, diffusional mixing is easier to perform due to molecular motion and self-diffusion. The activation energy of diffusion measured at the surface was  $E_{a\text{ surface}} = 14 \pm 2 \text{ kJ mol}^{-1}$ , whereas in the bulk it was  $E_{a\text{ bulk}} = 71 \pm 4 \text{ kJ mol}^{-1}$  (110, 111). Thus, diffusion at the surface is more significant than in bulk at 100–140 K. This finding indicates higher mobility on the surfaces and demonstrates that reaction preferentially occurs on ice surfaces, rather than in the bulk, at low temperatures.

The transport of protons or hydroxyl ions through ice is a fundamental phenomenon in physical chemistry. Both protons and hydroxyl ions are likely to stay at the surfaces (112, 113). One proton transport experiment involved the deposition of  $H_2O$  onto a  $D_2O$  layer; the excess protons were generated from HCl ionization at the interfaces. At low temperatures (<120 K), molecular motion was frozen, and proton or hydroxyl ion transport occurred by a proton hopping (Grötthuss) mechanism; molecular reorientation required relatively higher temperatures (100). The same research group also carried out a similar experiment with hydroxyl ions generated by sodium hydrolysis (113). The surface affinity of protons or hydroxyl ions can be used to study catalytic

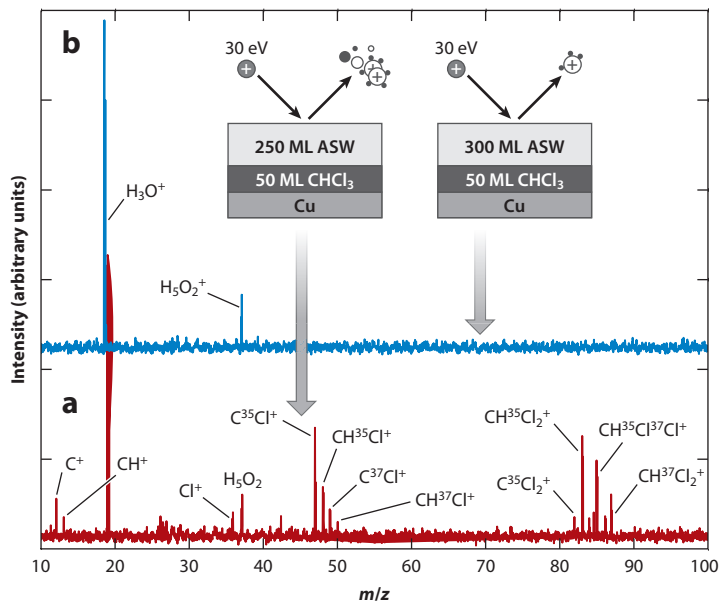


**Figure 3**

Spectra showing the difference in diffusive mixing between  $\text{CHCl}_3$  molecules at two different coverages of amorphous ice (ASW): (a) 250 and (b) 300 monolayers (ML). At 300 ML, the diffusive mixing of  $\text{CHCl}_3$  molecules stops; the spectrum contains only  $\text{H}_3\text{O}^+$  and  $(\text{H}_2\text{O})\text{H}_3\text{O}^+$  peaks. At 250 ML, all the peaks arising from the  $\text{CHCl}_3$  molecules are present. Reproduced with permission from Reference 53. Copyright 2007, American Chemical Society.

reactions on ice surfaces. A more recent study revealed the asymmetric transport of hydronium and hydroxyl ions through an ASW surface at low temperatures ( $<100$  K) (78).

Hyperthermal energy  $\text{Ar}^+$  ion scattering and sputtering are other important tools to explore the chemistry that occurs at the very top surface of molecular solids. Diffusion of small molecules such as chloromethanes and their interaction with ice have been investigated with hyperthermal energy  $\text{Ar}^+$  ion sputtering (53). In this study, different chloromethane molecules were deposited on a polycrystalline copper substrate, followed by water ice deposition; the  $\text{Ar}^+$  ion sputtering experiment was then performed in the temperature range between 110 and 150 K. The results showed that various chloromethane molecules diffuse at different rates through ASW. In the case of  $\text{CCl}_4$  molecules, diffusive mixing was almost completely precluded, whereas other chloromethane molecules diffused easily through ASW. **Figure 3** shows the diffusive mixing of  $\text{CHCl}_3$  molecules. When 250 monolayers [one monolayer comprises  $\sim 10^{15}$  molecules  $\text{cm}^{-2}$  (114)] of ASW were deposited on 50 monolayers of  $\text{CHCl}_3$  molecules, the sputtering spectra showed  $\text{CHCl}_3$  peaks, along with  $\text{H}_3\text{O}^+$  peaks. However, for 300 monolayers of ASW, only  $\text{H}_3\text{O}^+$  and  $\text{H}_5\text{O}_2^+$  peaks were present, implying that  $\text{CHCl}_3$  molecules can diffuse through 250 monolayers of ASW, whereas  $\text{CCl}_4$  molecules can diffuse through only 4 monolayers. The interaction energies between the chloromethanes and ASW are, in order,  $\text{CH}_3\text{Cl} > \text{CH}_2\text{Cl}_2 > \text{CHCl}_3 > \text{CCl}_4$ —the reverse of what occurs in the liquid-phase interaction.

The interaction between *n*-butanol (NBA) and ice has also been studied. NBA diffused through 1,000 monolayers of ASW, but water did not diffuse through 5 monolayers of NBA (47). Another study of the interaction between carboxylic acids—specifically, formic acid, acetic acid, and propionic acid—and water ice demonstrated structural reorientation and a strong interaction between

acetic acid and formic acid and water ice, which led to the formation of oligomers. Propionic acid did not strongly interact with the water ice (52).

### 3.3. Molecular Reaction/Interaction

Hyperthermal energy ions are useful for the study of reactions on surfaces and for the production of surface modifications. A recent investigation of ultralow-energy (1-eV) proton collisions on ice surfaces revealed that  $\text{H}_2^+$  ions formed from the surfaces (9). **Figure 4** shows the formation of  $\text{H}_2^+$  ions from  $\text{H}_2\text{O}$  after collision of 2-eV  $\text{H}^+$  ions, as well as the results from 1-eV collisions.  $\text{H}_2^+$  ion formation was more efficient in the case of ASW than with CW (9) because of the presence of greater numbers of dangling  $-\text{OH}$  bonds on ASW. This reaction has implications for interstellar chemistry and plasma-etching processes. A molecular dynamics study of proton collision on CW revealed proton reflection and collision-induced water desorption at low incident energies (0.05–4 eV) (72).

The reaction of small molecules such as CO (34),  $\text{CO}_2$  (115),  $\text{SO}_2$  (77), and  $\text{NO}_2$  (116); hydrolysis of sodium (117); and ionization of HCl molecules (18) have been studied on ice surfaces. The reaction between small molecules on ice surfaces is important in the context of atmospheric and environmental science. Hydrolysis of sodium produces  $\text{Na}^+$  and  $\text{OH}^-$  ions on ice surfaces; the latter tend to reside on the ice surfaces, whereas the former migrate into the bulk (117).

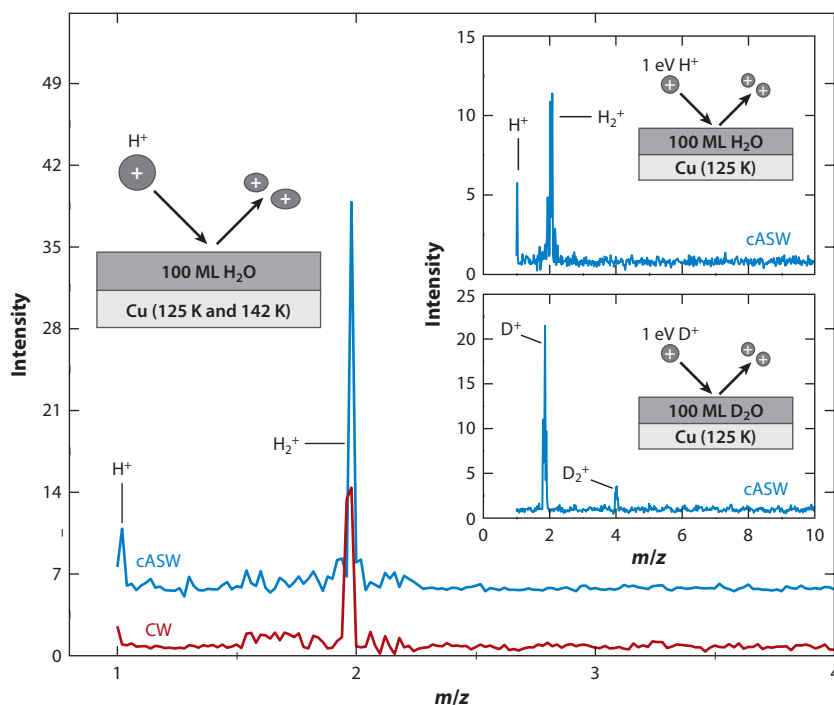


**Figure 4**

Mass spectrum generated after bombardment of 2-eV  $\text{H}^+$  ions on compact amorphous ice (cASW) and crystalline ice (CW). The spectrum from cASW is shifted vertically for clarity. (*Top inset*) The result of collision of 1-eV  $\text{H}^+$  ions on cASW and  $\text{D}^+$  ions on condensed  $\text{D}_2\text{O}$ , respectively, at 125 K. (*Bottom inset*) A simplification of the experiment shown in the top inset. Abbreviation: ML, monolayers. Reproduced with permission from Reference 9. Copyright 2011, American Chemical Society.

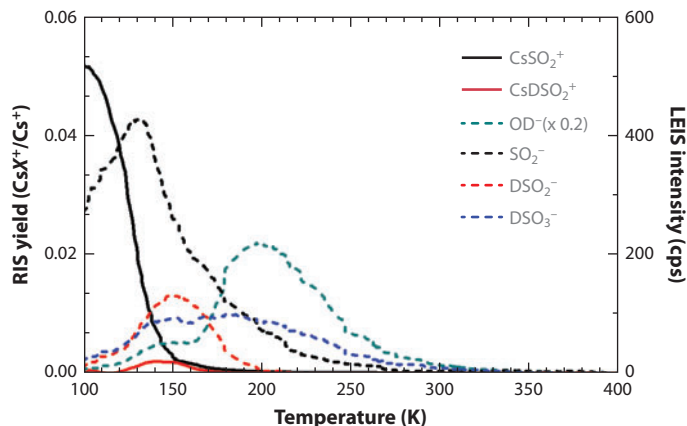


**Figure 5**

Temperature-programmed low-energy ion scattering (LEIS) measurements for signals of interest detected on the surface of a  $D_2O$ -ice film exposed to 0.3 Langmuir of  $SO_2$  at 80 K. The reactive ion scattering (RIS) yield on the left ordinate is the ratio of the LEIS product to the  $Cs^+$  signal intensity ( $CsX^+/Cs^+$ , where  $X$  is a neutral molecule on the surface). The appearance of  $CsSO_2^+$  and  $CsDSO_2^+$  signals in LEIS indicates the presence of  $SO_2$  and  $DSO_2$  species, respectively, on the surface. Other LEIS signals observed on the surface include  $OD^-$ ,  $SO_2^-$ ,  $DSO_2^-$ , and  $DSO_3^-$ . The temperature ramping rate was  $1\text{ K s}^{-1}$ . Reproduced with permission from Reference 77. Copyright 2009, American Chemical Society.

$CO_2$  interaction on ice films in both neutral and basic conditions did not yield any  $CO_2$ -water complexes or hydrolysis products in the temperature range between 80 and 180 K. Sufficient hydrogen bonding between  $OH^-$  ions and the ice surface suppressed the ions' reactivity toward  $CO_2$  (115).  $NO_2$  adsorbs molecularly on ice surfaces at 90 K and readily converts to HONO following heating at 140 K (116). This finding implies that the heterogeneous hydrolysis of  $NO_2$  is an important source of HONO formation. Efficient hydrolysis of  $NO_2$  at ice surfaces suggests that the corresponding atmospheric reaction will be facile at the surfaces of water films, aerosols, and icy particles.

A combination of hyperthermal ion collision and TPD has been used to investigate the interaction of  $SO_2$  and water ice at temperatures above 80 K. **Figure 5** shows the evolution of different chemical species, measured from a  $D_2O$  film adsorbed with  $SO_2$  through temperature-programmed LEIS (5). The authors of this study identified three types of intermediate chemical species, including a solvated  $SO_2$  species with a partial negative charge, a partially charged  $DSO_2$  species, and a strongly ionic  $DSO_3$ -like species (77). Efficient formation of these species at low temperatures indicates that the reaction involves a low energy barrier.

$H_2SO_4$  formation has also been observed through the deposition of  $H_2O$  and  $SO_3$  in different proportions (77). Interactions between molecules such as  $Cl_2$  (118),  $Cl_2O$  (118), and  $ClONO_2$  (2, 119), which are relevant to polar stratospheric clouds, have been studied on ice surfaces with static secondary ion mass spectrometry (SIMS) (119). The interaction between  $Cl_2$  and ice was minimal at 90 K. The  $Cl_2$  molecules and water reacted following heating to 130 K, which produced a mixed film of water, HClO, and solvated HCl (118). Unlike  $Cl_2$ ,  $Cl_2O$  did not react with water ice at 90 K; it showed only a hydrogen bond-like interaction at 130 K (118).  $ClONO_2$  deposited on pure water ice began to desorb at 120 K without any reaction, but in the presence of HCl it reacted promptly above 120 K and formed  $NO_3^-$  ions, providing evidence for the formation of  $HNO_3$  adsorbate (119).

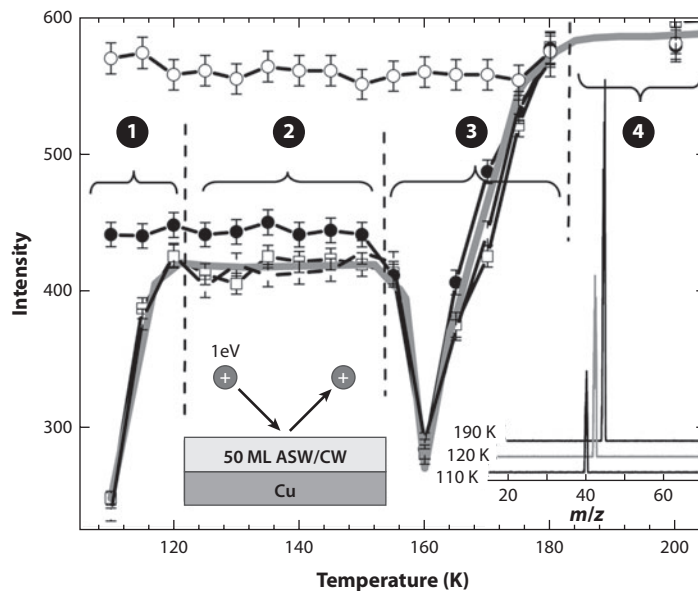


**Figure 6**

Plot of  $\text{Ar}^+$  ion scattering intensity versus temperature variation on various ice surfaces. The ion scattering intensity on a bare copper (Cu) surface is indicated by open circles, on 50 monolayers (ML) of amorphous ice (ASW;  $\text{H}_2\text{O}$ ) by open squares, on 50 ML of ASW ( $\text{D}_2\text{O}$ ) by filled squares, and on 50 ML of crystalline ice (CW;  $\text{H}_2\text{O}$ ) by filled circles. Comparing the ion scattering intensities of these four surfaces shows that the phase transition can be probed with the ultralow-energy ion/surface collision technique. (*Inset*) Typical 1-eV  $\text{Ar}^+$  ion scattering mass spectra of 50 ML of ASW for three different temperatures, averaged for 50 scans. Reproduced with permission from Reference 120. Copyright 2008, American Chemical Society.

### 3.4. The Phase Transition

The phase transition of thin ice films can be studied with different spectroscopic or spectrometric techniques. Two techniques are discussed here.

At IIT Madras (53), ultralow-energy ion scattering was used to probe a phase transition that occurs at approximately 120 K. ASW and CW films were formed on a copper surface, and an ultralow-energy ion scattering experiment was performed as a function of temperature. The result (**Figure 6**) compares the 1-eV  $\text{Ar}^+$  ion scattering intensity variation on ASW, with respect to CW. The transformation from ASW to CW is evident at 120 K but was irreversible because the ion scattering intensity did not change when the temperature was lowered from 150 K to 110 K. When the kinetic energy of the impinging ions was increased to 8 eV, the ions were unable to “identify” the structural change on the ice film. Therefore, ultralow-energy ions in the range between 1 and 3 eV should be used for such experiments because, in the ultralow-energy regime, collision of ions with surfaces depends on two factors: the translational energy of the projectile and its potential energy. At 110 K, ice surfaces have a porous structure that disappears at 120 K due to surface reorganization. Thus, trapping and the possibility of neutralization decrease, and the ion scattering intensity in this window increases (**Figure 6**). Moreover, the surface work function varies among different surfaces. CW has a 0.3 eV–higher work function than that of ASW (2.45 eV) (120). The structural transformation from ASW to CW reduces  $-\text{OH}$  dangling bonds and increases the work function. This change affects the scattering intensity of noble-gas ions, and structural transformations on the surfaces can be identified. In region 2 (120–155 K)

the intensity remains constant because no further change occurs, and in region 3 (155–180 K), desorption causes neutralization of the incoming ions through interaction with desorbing water molecules. Thereafter, the bare copper surface is presented to the incoming ions. This behavior can be verified with appropriate surfaces.

Other investigators used another important technique, temperature-programmed TOF-SIMS, to study phase transition in a series of molecular solids. They studied glass transition ( $T_g$ ) and film morphology changes in various molecular solids, such as water, methanol, ethanol, and 3-methyl pentane, on different metallic and nonmetallic surfaces. The  $T_g$  of vapor-deposited water ice occurred at 136 K, at which temperature water is transformed into a glassy solid (121). However, other reports indicate that the  $T_g$  of water is 165 K (122). This study revealed that intermixing of isotopically labeled water ice occurs at 136 K and that a film morphology change takes place at 165 K (122).

Apart from that of water ice, the  $T_g$  of methanol has been investigated in detail. The results showed that the  $T_g$  of vapor-deposited methanol films begins at 80 K, which is 23 K lower than its calorimetric  $T_g$  (22). In addition to water and alcohol, *n*-alkanes with no apparent  $T_g$  have also been studied. *n*-Pentane shows translational diffusion before crystallization (123). The translational diffusion in the film indicates that a liquid-like phase may appear immediately before crystallization. Another interesting aspect of such films is that they form droplets after crystallization, and their dewetting temperature depends on their initial thickness (86).

The presence of the liquid-like phase in water ice films has also been investigated. The liquid-like phase (or supercooled water) is important because it can be an extension of liquid water. Its presence in an ice film can be demonstrated in various ways (124), including by observation of the interaction between alkyl halide salts (e.g., LiCl, LiI, and NaCl) and ASW. A drastic increase in the solubility of these salts is expected to occur in supercooled water versus CW because the dissolution of salts into CW is suppressed (125–128). This solubility difference revealed that, above 136 K and below crystallization temperature, there is a phase similar to liquid water, known as the supercooled water phase, wherein molecules have long-range translational diffusion. In this phase, alkali halide salts dissolve. The existence of this phase is limited to the temperature range between 160 and 165 K (127). A further study confirmed that ASW is likely to transform into low-density liquid (LDL) above 136 K, and then to high-density liquid (HDL or supercooled liquid), prior to crystallization. This finding implies that glassy water shows polymorphism, that is, the presence of two distinct phases (129). Interestingly, the LDL is considered ultraviscous because of the lower solubility of alkali halide salts. The transition from LDL to HDL takes place at 160 K (130). Similar to water, molecular solids such as ethanol also showed polymorphism when vapor-deposited. An investigation involving the solubility of LiI in ethanol ice revealed the appearance of the liquid-like phase at 97 K and the crystalline phase at 130 K (131). Another molecular solid, toluene, shows self-diffusion and dewetting at 105 K and 117 K, respectively (132).

The effect of substrate on  $T_g$  values has also been explored. The  $T_g$  values of thin films are expected to be lower than bulk  $T_g$  values because of the nanoconfinement effect, which is similar to the lowering of melting point of such confined crystallites (86, 133, 134). To observe the substrate and the free-surface effect on the  $T_g$  value of ASW, investigators vapor-deposited water at 120 K on graphite and other ionic liquids (131). Self-diffusion and film morphology changes were observed in the deposited ice film; these effects arise from instability at the graphite interface. Dewetting of up to 20 monolayers of water was observed on the hydrophobic graphite surface. A similar effect on Ni(111) was not observed because of the presence of a so-called dead layer at the interface between the metal surface and the ice (135).

### 3.5. Soft Landing and Its Applications in Organometallics

In soft landing, polyatomic ions whose energy is between 10 and 20 eV are deposited intact onto a target surface (82). The ions are not neutralized in this process. Without breaking the covalent bond, the polyatomic ions dissipate the kinetic energy during impact, and the dissipated energy changes the vibrational and electronic energy of the surface and the polyatomic ions. Soft-landing experiments play an important role in the fields of materials science, engineering, catalysis, nanotechnology, and biology (86). In 1977, the Cooks group became the first to conduct a soft-landing experiment (75). In another early study, positively charged organic ions prepared from desorption/ionization were landed on a target surface (136). In subsequent soft-landing experiments,  $(\text{CH}_3)_2\text{SiNCS}^+$  ions, *N,N*-dimethyl-*p*-toluidine ions, and *m*-trifluoromethylbenzoyl ions were collided separately on a fluorinated SAM or a long-chain alkyl SAM (H-SAM) (82, 137, 138). The release of projectiles from the SAMs following chemical sputtering illustrates the nondestructive nature of this process.

Soft landing has been used in organometallics; here, metal complex molecules are produced in the gas phase, then gently landed onto the desired surface without any change or rupture of the chemical bond. Complex molecules that are difficult to synthesize in solution chemistry are often used in such cases. Metal-benzene and metal-salen [salen refers to *N,N'*-ethylenebis(salicylideneaminato)] are common organometallic compounds used in soft-landing experiments (139, 140). Nakajima and colleagues (139) produced  $\text{V}(\text{benzene})^+$  and  $\text{V}_n(\text{benzene})_{n+1}$  ions (known as multidecker sandwich cluster ions) by laser evaporation, followed by soft landing onto an argon matrix prepared on polycrystalline gold surfaces at 18 K. Subsequent IR surface analysis revealed the nondissociative deposition of the desired ions on the surface.

In other studies, ions of transition metals such as titanium, scandium, and chromium were deposited at room temperature onto different SAMs (141, 142). The collision energy ranged between 10 and 20 eV. The soft-landed molecules on the SAMs were stable because the desorption energy calculated from the TPD experiments was high (143). These experiments were performed with  $\text{V}_2(\text{benzene})_3^+$  multidecker complex ions, which were landed onto a 1-octadecanethiol SAM at a kinetic energy of approximately 20 eV (143, 144). A TPD experiment on the soft-landed surface showed the presence of  $\text{V}(\text{benzene})_2$  and the  $\text{V}_2(\text{benzene})_2$  molecules on the surface. These molecules may have arisen from dissociation during landing on the SAM and may subsequently have become immobilized in the SAM layer (Figure 7) (86).

The trapping of soft-landed ions depends on the density of the SAMs. SAMs prepared on gold are well ordered and more densely populated than those on silicon. Therefore, the desorption energy of  $\text{V}(\text{benzene})$ -complex ions from a  $\text{C}_{16}$ -SAM prepared on Si(111) is much lower than that of a  $\text{C}_{16}$ -SAM prepared on Au(111) (142). The orientation of the molecules following landing depends on the nature of the SAM. The molecular axis of  $\text{V}(\text{benzene})_2$  molecules in the H-SAM substrate remains at 70–80° with respect to the surface normal (141). The molecular orientation of other complexes [ $M(\text{benzene})_2$ ;  $M = \text{Ti}$  or  $\text{Cr}$ ] shows a similar trend, although chromium-complex molecules have a lower-than-70° angle with respect to the surface normal (144). However, in the case of F-SAM surfaces, the angles differ because of the repulsion between the  $\pi$ -electron cloud of the benzene ring of the complex and the closest outermost  $-\text{CF}_3$  and  $-\text{CF}_2$  groups on the side chain of the fluorocarbon axes of the F-SAM (86).

The reactivity of the complex cations landed on the SAM was subsequently investigated in detail.  $\text{VO}(\text{salen})^+$  and  $[\text{Ni}(\text{salen})+\text{H}]^+$  ions were produced by electrospray ionization and, after mass selection, were allowed to soft-land onto an F-SAM on gold (145). The TOF-SIMS analysis, performed over 4 days following deposition, caused the reduction of  $\text{V}^{\text{V}}\text{O}(\text{salen})^+$  to  $\text{V}^{\text{III}}(\text{salen})^+$ . This result indicates that the reduction was interfacial, not beam induced. However, the yield of

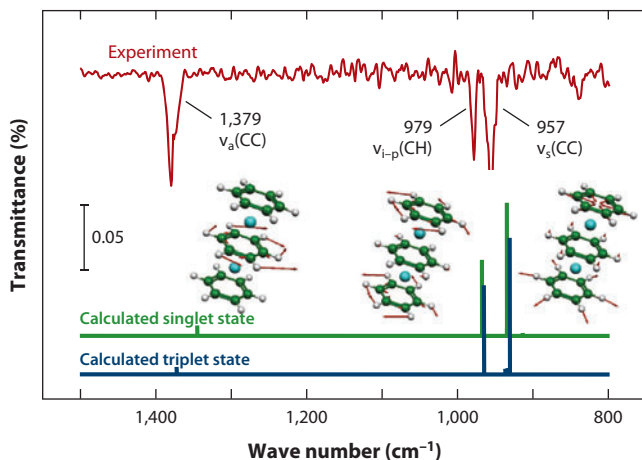


**Figure 7**

The IR spectrum in the range between 800 and 1,500  $\text{cm}^{-1}$  recorded after the soft landing of approximately one monolayer of  $\text{V}_2(\text{benzene})_3$  ions ( $2 \times 10^{14}$  positive ions  $\text{cm}^{-2}$ ) at 200 K onto a 1-octadecanethiol monolayer, along with the computed IR spectra of the singlet and triplet states of  $\text{V}_2(\text{benzene})_3$  ions. The labels  $\nu_s(\text{CC})$ ,  $\nu_{i-p}(\text{CH})$ , and  $\nu_a(\text{CC})$  stand for the symmetric breathing mode of two terminal benzene rings, the in-plane bending mode of these benzene rings, and the asymmetric C–C stretching mode of the central ring, respectively. Reproduced with permission from Reference 86. Copyright 2012, American Chemical Society.

$\text{V}^{\text{III}}(\text{salen})^+$  ions depended on the nature of the proton donor molecule needed for the reaction and its residence time on the surface (145). In the reverse reaction,  $\text{V}^{\text{III}}(\text{salen})^+$  was easily converted to  $\text{V}^{\text{V}}\text{O}(\text{salen})^+$ . This catalytic cycle of reduction and oxidation by a soft-landed vanadium complex depended on two factors: the initial number of the proton source molecules and the rate of release of the protons from the proton donor molecules (86).

#### 4. SUMMARY AND FUTURE DIRECTIONS

The selected examples presented in this review, although they offer merely glimpses into an exciting area, establish that many exciting areas of research have yet to be explored. Ultrahigh surface sensitivity that can cause molecular transformations, extract chemical information, preserve ionic species, and accommodate functional moieties—all in a spatially controlled fashion—is the most fascinating aspect of such research. Completely new phenomena are expected to be discovered on solids that have not yet been investigated.

One as-yet-unexplored research avenue involves catalysis at molecular solids. Another pertains to the dynamics of events, which would probably be best explored with pulsed ion beams. All such investigations can generate complete information only in conjunction with computational studies, which can probe ultrafast dynamics. The development of techniques in this area would enrich experimental efforts. From the experimental point of view, all these new approaches would require new instrumentation with high transmission at low energies and high detector sensitivity. Experiments on many molecular solids require temperatures lower than what can be attained with liquid nitrogen. Given these diverse requirements, LEIS as an analytical tool will become more instrumentation intensive during the coming years. Experimental curiosity and possible new phenomena are likely to propel research in this area.

## DISCLOSURE STATEMENT

The authors are not aware of any affiliations, memberships, funding, or financial holdings that might be perceived as affecting the objectivity of this review.

## ACKNOWLEDGMENTS

T.P. acknowledges the Department of Science and Technology, Government of India, for funding. S.B. and R.G.B. acknowledge the Council of Scientific and Industrial Research for research fellowships.

## LITERATURE CITED

1. Molina MJ, Rowland FS. 1974. Stratospheric sink for chlorofluoromethanes: chlorine atom-catalysed destruction of ozone. *Nature* 249:810–12
2. Molina MJ, Tso T-L, Molina LT, Wang FCY. 1987. Antarctic stratospheric chemistry of chlorine nitrate, hydrogen chloride, and ice: release of active chlorine. *Science* 238:1253–57
3. Salcedo D, Molina LT, Molina MJ. 2001. Homogeneous freezing of concentrated aqueous nitric acid solutions at polar stratospheric temperatures. *J. Phys. Chem. A* 105:1433–39
4. Thiel PA, Madey TF. 1987. The interaction of water with solid surfaces: fundamental aspects. *Surf. Sci. Rep.* 7:211–385
5. Park S-C, Moon E-S, Kang H. 2010. Some fundamental properties and reactions of ice surfaces at low temperatures. *Phys. Chem. Chem. Phys.* 12:12000–11
6. Haq S, Clay C, Darling GR, Zimbitas G, Hodgson A. 2006. Growth of intact water ice on Ru(0001) between 140 and 160 K: experiment and density-functional theory calculations. *Phys. Rev. B* 73:115414
7. Hodgson A, Haq S. 2009. Water adsorption and the wetting of metal surfaces. *Surf. Sci. Rep.* 64:381–451
8. Kimmel GA, Petrik NG, Dohnalek Z, Kay BD. 2007. Crystalline ice growth on Pt(111) and Pd(111): nonwetting growth on a hydrophobic water monolayer. *J. Chem. Phys.* 126:114702
9. Bag S, McCoustra MRS, Pradeep T. 2011. Formation of  $H_2^+$  by ultra-low-energy collisions of protons with water ice surfaces. *J. Phys. Chem. C* 115:13813–19
10. Materer N, Starke U, Barbieri A, Van Hove MA, Somorjai GA, et al. 1997. Molecular surface structure of ice(0001): dynamical low-energy electron diffraction, total-energy calculations and molecular dynamics simulations. *Surf. Sci.* 381:190–210
11. Braun J, Glebov A, Graham AP, Menzel A, Toennies JP. 1998. Structure and phonons of the ice surface. *Phys. Rev. Lett.* 80:2638–41
12. Glebov A, Graham AP, Menzel A, Toennies JP, Senet P. 2000. A helium atom scattering study of the structure and phonon dynamics of the ice surface. *J. Chem. Phys.* 112:11011–22
13. Materer N, Starke U, Barbieri A, Van Hove MA, Somorjai GA, et al. 1995. Molecular surface structure of a low-temperature ice Ih(0001) crystal. *J. Phys. Chem.* 99:6267–69
14. Biesecker JP, Ellison GB, Wang H, Iedema MJ, Tsekouras AA, Cowin JP. 1998. Ion beam source for soft-landing deposition. *Rev. Sci. Instrum.* 69:485–95
15. Tsekouras AA, Iedema MJ, Cowin JP. 1999. Soft-landed ion diffusion studies on vapor-deposited hydrocarbon films. *J. Chem. Phys.* 111:2222–34
16. Bolina AS, Wolff AJ, Brown WA. 2005. Reflection absorption infrared spectroscopy and temperature-programmed desorption studies of the adsorption and desorption of amorphous and crystalline water on a graphite surface. *J. Phys. Chem. B* 109:16836–45
17. Engquist I, Lundström I, Liedberg B. 1995. Temperature-programmed desorption and infrared studies of  $D_2O$  ice on self-assembled alkanethiolate monolayers: influence of substrate wettability. *J. Phys. Chem.* 99:12257–67
18. Park S-C, Kang H. 2005. Adsorption, ionization, and migration of hydrogen chloride on ice films at temperatures between 100 and 140 K. *J. Phys. Chem. B* 109:5124–32

19. Smith RS, Huang C, Wong EKL, Kay BD. 1997. The molecular volcano: abrupt  $\text{CCl}_4$  desorption driven by the crystallization of amorphous solid water. *Phys. Rev. Lett.* 79:909–12
20. Sadtchenko V, Knutsen K, Giese CF, Gentry WR. 2000. Interactions of  $\text{CCl}_4$  with thin  $\text{D}_2\text{O}$  amorphous ice films. Part I. A nanoscale probe of ice morphology. *J. Phys. Chem. B* 104:2511–21
21. McClure SM, Barlow ET, Akin MC, Safarik DJ, Truskett TM, Mullins CB. 2006. Transport in amorphous solid water films: implications for self-diffusivity. *J. Phys. Chem. B* 110:17987–97
22. Souda R. 2004. Glass transition and intermixing of amorphous water and methanol. *Phys. Rev. Lett.* 93:235502
23. Kondo T, Kato HS, Bonn M, Kawai M. 2007. Deposition and crystallization studies of thin amorphous solid water films on Ru(0001) and on CO-precovered Ru(0001). *J. Chem. Phys.* 127:094703
24. Borget F, Chivassa T, Allouche A, Marinelli F, Aycard JP. 2001. Cyanoacetylene adsorption on amorphous and crystalline water ice films: investigation through matrix isolation and quantum study. *J. Am. Chem. Soc.* 123:10668–75
25. Burke DJ, Wolff AJ, Edridge JL, Brown WA. 2008. Thermally induced mixing of water dominated interstellar ices. *Phys. Chem. Chem. Phys.* 10:4956–67
26. Faradzhev NS, Perry CC, Kusmierek DO, Fairbrother DH, Madey TE. 2004. Kinetics of electron-induced decomposition of  $\text{CF}_2\text{Cl}_2$  coadsorbed with water (ice): a comparison with  $\text{CCl}_4$ . *J. Chem. Phys.* 121:8547–61
27. Graham JD, Roberts JT. 1995. Interaction of HCl with crystalline and amorphous ice: implications for the mechanisms of ice-catalyzed reactions. *Geophys. Res. Lett.* 22:251–54
28. Schaff JE, Roberts JT. 1994. Structure sensitivity in the surface chemistry of ice: acetone adsorption on amorphous and crystalline ice films. *J. Phys. Chem.* 98:6900–2
29. Schaff JE, Roberts JT. 1996. Toward an understanding of the surface chemical properties of ice: differences between the amorphous and crystalline surfaces. *J. Phys. Chem.* 100:14151–60
30. Schaff JE, Roberts JT. 1998. The adsorption of acetone on thin films of amorphous and crystalline ice. *Langmuir* 14:1478–86
31. Callen BW, Griffiths K, Norton PR. 1992. Observation of free hydroxyl groups on the surface of ultra thin ice layers on nickel(110). *Surf. Sci.* 261:L44–L48
32. Henderson MA. 2002. The interaction of water with solid surfaces: fundamental aspects revisited. *Surf. Sci. Rep.* 46:1–308
33. Hu Y, Griffiths K. 2007. NO–methanol interaction on the surface of Pt(332). *Surf. Sci.* 601:2467–72
34. Hu Y, Norton PR, Griffiths K. 2007. CO– $\text{D}_2\text{O}$  coadlayers on Pt(111). Vibrational studies at low coverages. *J. Vac. Sci. Technol. A* 25:645–50
35. Maté B, Medialdea A, Moreno MA, Escribano R, Herrero VJ. 2003. Experimental studies of amorphous and polycrystalline ice films using FT-RAIRS. *J. Phys. Chem. B* 107:11098–108
36. Maté B, Rodriguez-Lazcano Y, Herrero VJ. 2012. Morphology and crystallization kinetics of compact (HGW) and porous (ASW) amorphous water ice. *Phys. Chem. Chem. Phys.* 14:10595–602
37. Mitlin S, Leung KT. 2002. Film growth of ice by vapor deposition at 128–185 K studied by Fourier transform infrared reflection–absorption spectroscopy: evolution of the OH stretch and the dangling bond with film thickness. *J. Phys. Chem. B* 106:6234–47
38. Buch V, Devlin JP. 1991. Spectra of dangling OH bonds in amorphous ice: assignment to 2- and 3-coordinated surface molecules. *J. Chem. Phys.* 94:4091–92
39. Buch V, Milet A, Vacha R, Jungwirth P, Devlin JP. 2007. Water surface is acidic. *Proc. Natl. Acad. Sci. USA* 104:7342–47
40. Delzeit L, Rowland B, Devlin JP. 1993. Infrared spectra of hydrogen chloride complexed/ionized in amorphous hydrates and at ice surfaces in the 15–90 K range. *J. Phys. Chem.* 97:10312–18
41. Devlin JP, Joyce C, Buch V. 2000. Infrared spectra and structures of large water clusters. *J. Phys. Chem. A* 104:1974–77
42. Devlin JP, Uras N, Sadlej J, Buch V. 2002. Discrete stages in the solvation and ionization of hydrogen chloride adsorbed on ice particles. *Nature* 417:269–71
43. Rowland B, Fisher M, Devlin JP. 1991. Probing icy surfaces with the dangling-OH-mode absorption: large ice clusters and microporous amorphous ice. *J. Chem. Phys.* 95:1378–84

44. Rowland B, Kadagathur NS, Devlin JP, Buch V, Feldman T, Wojcik MJ. 1995. Infrared spectra of ice surfaces and assignment of surface-localized modes from simulated spectra of cubic ice. *J. Chem. Phys.* 102:8328–41
45. Graham JD, Roberts JT. 1994. Interaction of hydrogen chloride with an ultrathin ice film: observation of adsorbed and absorbed states. *J. Phys. Chem.* 98:5974–83
46. Blanchard JL, Roberts JT. 1994. Interaction of  $\text{CCl}_4$  with the surface of amorphous ice. *Langmuir* 10:3303–10
47. Kumar GN, Cyriac J, Bag S, Pradeep T. 2009. Low energy ion scattering investigations of *n*-butanol-ice system in the temperature range of 110–150 K. *J. Phys. Chem. C* 113:14258–63
48. Cooks RG, Ast T, Pradeep T, Wysocki V. 1994. Reactions of ions with organic surfaces. *Acc. Chem. Res.* 27:316–23
49. Kang H. 2011. Reactive ion scattering of low energy  $\text{Cs}^+$  from surfaces. A technique for surface molecular analysis. *Bull. Korean Chem. Soc.* 32:389–98
50. Ullah S, Dogar AH, Qayyum A. 2011. Surface-induced dissociation of low energy  $\text{H}_2^+$  impact on a carbon surface: a Monte Carlo simulation. *Commun. Theor. Phys.* 55:315–20
51. Feketeova L, Zabka J, Zappa F, Grill V, Scheier P, et al. 2009. Surface-induced dissociation and chemical reactions of  $\text{C}_2\text{D}_4^+$  on stainless steel, carbon (HOPG), and two different diamond surfaces. *J. Am. Soc. Mass Spectrom.* 20:927–38
52. Cyriac J, Pradeep T. 2008. Interaction of carboxylic acids and water ice probed by argon ion induced chemical sputtering. *J. Phys. Chem. C* 112:1604–11
53. Cyriac J, Pradeep T. 2007. Probing difference in diffusivity of chloromethanes through water ice in the temperature range of 110–150 K. *J. Phys. Chem. C* 111:8557–65
54. Rezaat T, Shukla A. 2007. Dissociative scattering of hyperthermal energy  $\text{CF}_3^+$  ions from modified surfaces. *J. Chem. Phys.* 126:084701
55. Kim JH, Lahaye RJWE, Kang H. 2007. Evidence for Eley–Rideal abstraction mechanism in reactive ion scattering of  $\text{Cs}^+$  from Pt(111) adsorbed with CO and  $\text{CO}_2$ . *Surf. Sci.* 601:434–40
56. Levandier DJ, Chiu Y-H, Dressler RA, Sun L, Schatz GC. 2004. Hyperthermal reactions of  $\text{O}^+(\text{S}_{3/2})$  with  $\text{CD}_4$  and  $\text{CH}_4$ : theory and experiment. *J. Phys. Chem. A* 108:9794–804
57. Levandier DJ, Chiu Y-H, Dressler RA. 2004. Reactions of  $\text{O}^+$  with  $\text{C}_n\text{H}_{2n+2}$ ,  $n = 2-4$ : a guided ion beam study. *J. Chem. Phys.* 120:6999–7007
58. Wade N, Jo S-C, Gologan B, Cooks RG. 2003. Differentiation of isomeric oxygenated adsorbates using low-energy ion/surface collisions. *Int. J. Mass Spectrom.* 230:151–59
59. Laskin J, Futrell JH. 2003. Energy transfer in collisions of peptide ions with surfaces. *J. Chem. Phys.* 119:3413–20
60. Han SJ, Lee CW, Lahaye RJWE, Kang H. 2003. Hyperthermal scattering of  $\text{Cs}^+$  from Pt(111): the effect of image charge on the ion-surface energy transfer. *Surf. Sci.* 538:184–90
61. Lahaye RJWE, Kang H. 2003. Mechanism for the efficient abstraction of an adsorbate by  $\text{Cs}^+$  scattering at hyperthermal energies. *Phys. Rev. B* 67:033401
62. Shukla AK, Futrell JH. 2003. Dynamics of hyperthermal energy ion-surface collisions: dissociative and non-dissociative scattering of ethanol cations from a self-assembled monolayer surface of fluorinated alkyl thiol on Au(111). *Int. J. Mass Spectrom.* 223/224:783–801
63. Hahn JR, Lee CW, Han SJ, Lahaye RJWE, Kang H. 2002. Low-energy  $\text{Cs}^+$  scattering from water on Pt(111): a kinetic energy analysis of the  $\text{Cs}^+$ -water clusters. *J. Phys. Chem. A* 106:9827–31
64. Park S-C, Maeng K-W, Pradeep T, Kang H. 2001. Reactive ion scattering from pure and mixed HCl,  $\text{NH}_3$  and  $\text{D}_2\text{O}$  surfaces. *Nucl. Instrum. Methods B* 182:193–99
65. Grill V, Shen J, Evans C, Cooks RG. 2001. Collisions of ions with surfaces at chemically relevant energies: instrumentation and phenomena. *Rev. Sci. Instrum.* 72:3149–79
66. Gu C, Wysocki VH, Harada A, Takaya H, Kumadaki I. 1999. Dissociative and reactive hyperthermal ion-surface collisions with Langmuir–Blodgett films terminated by  $\text{CF}_3(\text{CH}_2)_n^-$ , *n*-perfluoroalkyl, or *n*-alkyl groups. *J. Am. Chem. Soc.* 121:10554–62
67. Wade N, Pradeep T, Shen J, Cooks RG. 1999. Covalent chemical modification of self-assembled fluorocarbon monolayers by low-energy  $\text{CH}_2\text{Br}_2^+$  ions: a combined ion/surface scattering and X-ray photoelectron spectroscopic investigation. *Rapid Commun. Mass Spectrom.* 13:986–93

68. Ada ET, Kornienko O, Hanley L. 1998. Chemical modification of polystyrene surfaces by low-energy polyatomic ion beams. *J. Phys. Chem. B* 102:3959–66
69. Hanley L, Lim H, Schultz DG, Wainhaus SB, de Sainte Claire P, Hase WL. 1997. Surface energy transfer by low energy polyatomic ion collisions. *Nucl. Instrum. Methods B* 125:218–22
70. Kang H, Kim KD, Kim KY. 1997. Molecular identification of surface adsorbates. Reactive scattering of hyperthermal  $\text{Cs}^+$  from a Ni(100) surface adsorbed with CO,  $\text{C}_6\text{H}_6$ , and  $\text{H}_2\text{O}$ . *J. Am. Chem. Soc.* 119:12002–3
71. Kang H, Yang MC, Kim KD, Kim KY. 1998. Reactive scattering of  $\text{Cs}^+$  from chemisorbed molecules on a Ni(100) surface. Secondary neutral mass spectrometry with a hyperthermal ion beam. *Int. J. Mass Spectrom. Ion Process.* 174:143–54
72. Sanfelix PC, Al-Halabi A, Darling GR, Holloway S, Kroes G-J. 2005. Protons colliding with crystalline ice: proton reflection and collision induced water desorption at low incidence energies. *J. Am. Chem. Soc.* 127:3944–51
73. Al-Halabi A, Sanfelix PC, Holloway S, Kroes G-J, Darling GR. 2006. Protons colliding with ice: bouncing, sticking, splashing. *Surf. Sci.* 600:4247–50
74. Cooks RG, Ast T, Mabud MA. 1990. Collisions of polyatomic ions with surfaces. *Int. J. Mass Spectrom. Ion Process.* 100:209–65
75. Franchetti V, Solka BH, Baitinger WE, Amy JW, Cooks RG. 1977. Soft landing of ions as a means of surface modification. *Int. J. Mass Spectrom. Ion Phys.* 23:29–35
76. Kang H. 2005. Chemistry of ice surfaces. Elementary reaction steps on ice studied by reactive ion scattering. *Acc. Chem. Res.* 38:893–900
77. Kim YK, Kim SK, Kim JH, Kang H. 2009. Kinetic isolation of reaction intermediates on ice surfaces. Precursor states of  $\text{SO}_2$  hydrolysis. *J. Phys. Chem. C* 113:16863–65
78. Moon E-S, Kim YK, Shin S, Kang H. 2012. Asymmetric transport efficiencies of positive and negative ion defects in amorphous ice. *Phys. Rev. Lett.* 108:226103
79. Volný M, Elam WT, Ratner BD, Turecek F. 2005. Preparative soft and reactive landing of gas-phase ions on plasma-treated metal surfaces. *Anal. Chem.* 77:4846–53
80. Wang P, Hadjar O, Gassman PL, Laskin J. 2008. Reactive landing of peptide ions on self-assembled monolayer surfaces: an alternative approach for covalent immobilization of peptides on surfaces. *Phys. Chem. Chem. Phys.* 10:1512–22
81. Johnson GE, Hu Q, Laskin J. 2011. Soft landing of complex molecules on surfaces. *Annu. Rev. Anal. Chem.* 4:83–104
82. Miller SA, Luo H, Pachuta SJ, Cooks RG. 1997. Soft-landing of polyatomic ions at fluorinated self-assembled monolayer surfaces. *Science* 275:1447–50
83. Ast T, Mabud MA, Cooks RG. 1988. Reactive collisions of polyatomic ions at solid surfaces. *Int. J. Mass Spectrom. Ion Process.* 82:131–50
84. Cristoni S, Rubini S, Bernardi LR. 2007. Development and applications of surface-activated chemical ionization. *Mass Spectrom. Rev.* 26:645–56
85. Sleno L, Volmer DA. 2004. Ion activation methods for tandem mass spectrometry. *J. Mass Spectrom.* 39:1091–112
86. Cyriac J, Pradeep T, Kang H, Souda R, Cooks RG. 2012. Low-energy ionic collisions at molecular solids. *Chem. Rev.* 112:5356–411
87. Kaplan A, Manor Y, Bekkerman A, Tsipinyuk B, Kolodney E. 2003. Implanting atomic ions into surface adsorbed fullerenes: the single collision formation and emission of  $\text{Cs}@C_{60}^+$  and  $\text{Cs}@C_{70}^+$ . *Int. J. Mass Spectrom.* 228:1055–65
88. Fernandez FM, Smith LL, Kuppanan K, Yang X, Wysocki VH. 2003. Peptide sequencing using a patchwork approach and surface-induced dissociation in sector-TOF and dual quadrupole mass spectrometers. *J. Am. Soc. Mass Spectrom.* 14:1387–401
89. Pradeep T, Riederer DE Jr, Hoke SH II, Ast T, Cooks RG, Linford MR. 1994. Reactions of metal ions at fluorinated SAM (self-assembled monolayer) surfaces: formation of  $\text{MF}_n^+$  ( $M = \text{Ti, Cr, Fe, Mo, and W; } n = 1-5$ ). *J. Am. Chem. Soc.* 116:8658–65
90. Maeno N, Ebinuma T. 1983. Pressure sintering of ice and its implication to the densification of snow at polar glaciers and ice sheets. *J. Phys. Chem.* 87:4103–10

91. Pritchard HD, Ligtenberg SRM, Fricker HA, Vaughan DG, van den Broeke MR, Padman L. 2012. Antarctic ice-sheet loss driven by basal melting of ice shelves. *Nature* 484:502–5
92. Prenni AJ, Tolbert MA. 2001. Studies of polar stratospheric cloud formation. *Acc. Chem. Res.* 34:545–53
93. Snow TP, Bierbaum VM. 2008. Ion chemistry in the interstellar medium. *Annu. Rev. Anal. Chem.* 1:229–59
94. Bouwman J, Paardekooper DM, Cuppen HM, Linnartz H, Allamandola LJ. 2009. Real-time optical spectroscopy of vacuum ultraviolet irradiated pyrene: H<sub>2</sub>O interstellar ice. *Astrophys. J.* 700:56–62
95. Gibb EL, Whittet DCB, Boogert ACA, Tielens AGGM. 2004. Interstellar ice. The infrared space observatory legacy. *Astrophys. J. Suppl.* 151:35–73
96. Pedersen C, Mihranyan A, Strømme M. 2011. Surface transition on ice induced by the formation of a grain boundary. *PLoS ONE* 6:e24373
97. Koop T, Kapilashrami A, Molina LT, Molina MJ. 2000. Phase transitions of sea-salt/water mixtures at low temperatures: implications for ozone chemistry in the polar marine boundary layer. *J. Geophys. Res.* 105:26393–402
98. Blomquist J, Andersson MP, Uvdal P. 2011. Inducing H/D exchange in ultrathin ice films by proton deficiency. *Phys. Rev. Lett.* 107:216101
99. Gálvez O, Maté B, Herrero VJ, Escribano R. 2011. HDO infrared detection sensitivity and D/H isotopic exchange in amorphous and crystalline ice. *Astrophys. J.* 738:133
100. Lee C-W, Lee P-R, Kim YK, Kang H. 2007. Mechanistic study of proton transfer and H/D exchange in ice films at low temperatures (100–140 K). *J. Chem. Phys.* 127:084701
101. Lu H, McCartney SA, Sadtchenko V. 2009. H/D exchange kinetics in pure and HCl doped polycrystalline ice at temperatures near its melting point: structure, chemical transport, and phase transitions at grain boundaries. *J. Chem. Phys.* 130:054501
102. Moon E-S, Yoon J, Kang H. 2010. Energy barrier of proton transfer at ice surfaces. *J. Chem. Phys.* 133:044709
103. Pan M, Pozun ZD, Yu W-Y, Henkelman G, Mullins CB. 2012. Structure revealing H/D exchange with co-adsorbed hydrogen and water on gold. *J. Phys. Chem. Lett.* 3:1894–99
104. Park S-C, Jung K-H, Kang H. 2004. H/D isotopic exchange between water molecules at ice surfaces. *J. Chem. Phys.* 121:2765–74
105. Souda R. 2005. TOF-SIMS analysis of ion-water interactions. *Nucl. Instrum. Methods B* 232:125–33
106. Weber AS, Hodyss R, Johnson PV, Willacy K, Kanik I. 2009. Hydrogen-deuterium exchange in photolyzed methane-water ices. *Astrophys. J.* 703:1030–33
107. Pachuta SJ, Cooks RG. 1987. Mechanisms in molecular SIMS. *Chem. Rev.* 87:647–69
108. Jacobs DC. 2002. Reactive collisions of hyperthermal energy molecular ions with solid surfaces. *Annu. Rev. Phys. Chem.* 53:379–407
109. Gologan B, Green JR, Alvarez J, Laskin J, Graham CR. 2005. Ion/surface reactions and ion soft landing. *Phys. Chem. Chem. Phys.* 7:1490–500
110. Jung K-H, Park S-C, Kim JH, Kang H. 2004. Vertical diffusion of water molecules near the surface of ice. *J. Chem. Phys.* 121:2758–64
111. Livingston FE, Whipple GC, George SM. 1997. Diffusion of HDO into single-crystal H<sub>2</sub><sup>16</sup>O ice multilayers: comparison with H<sub>2</sub><sup>18</sup>O. *J. Phys. Chem. B* 101:6127–31
112. Lee C-W, Lee P-R, Kang H. 2006. Protons at ice surfaces. *Angew. Chem. Int. Ed.* 45:5529–33
113. Kim S, Park E, Kang H. 2011. Segregation of hydroxide ions to an ice surface. *J. Chem. Phys.* 135:074703
114. Moon E-S, Kang H, Oba Y, Watanabe N, Kouchi A. 2010. Direct evidence for ammonium ion formation in ice through ultraviolet-induced acid-base reaction of NH<sub>3</sub> with H<sub>3</sub>O<sup>+</sup>. *Astrophys. J.* 713:906–11
115. Kim YK, Park S-C, Kim JH, Lee C-W, Kang H. 2008. Interaction of carbon dioxide and hydroxide ion at the surface of ice films. *J. Phys. Chem. C* 112:18104–9
116. Kim SK, Kang H. 2010. Efficient conversion of nitrogen dioxide into nitrous acid on ice surfaces. *J. Phys. Chem. Lett.* 1:3085–89
117. Kim JH, Kim YK, Kang H. 2008. Hydrolysis of sodium atoms on water-ice films: characterization of reaction products and interfacial distribution of sodium and hydroxide ions. *J. Phys. Chem. C* 113:321–27

118. Donsig HA, Herridge D, Vickerman JC. 1998. Static SIMS studies of reactions on mimics of polar stratospheric clouds. II. Low-temperature, low-pressure interactions of  $\text{Cl}_2$  and  $\text{Cl}_2\text{O}$  with solid ice films. *J. Phys. Chem. A* 102:2302–8
119. Donsig HA, Herridge D, Vickerman JC. 1999. Static SIMS studies of reactions on mimics of polar stratospheric clouds. III. Mechanism of chlorine nitrate decomposition and reaction. *J. Phys. Chem. A* 103:9211–20
120. Cyriac J, Pradeep T. 2008. Structural reorganization on amorphous ice films below 120 K revealed by near-thermal ( $\sim 1$  eV) ion scattering. *J. Phys. Chem. C* 112:5129–35
121. Johari GP, Hallbrucker A, Mayer E. 1987. The glass-liquid transition of hyperquenched water. *Nature* 330:552–53
122. Yue Y, Angell CA. 2004. Clarifying the glass-transition behavior of water by comparison with hyperquenched inorganic glasses. *Nature* 427:717–20
123. Souda R. 2009. Liquid-like nature of crystalline *n*-butane and *n*-pentane films studied by time-of-flight secondary ion mass spectrometry. *J. Phys. Chem. B* 113:15831–35
124. Jenniskens P, Banham SF, Blake DF, McCoustra MRS. 1997. Liquid water in the domain of cubic crystalline ice  $I_c$ . *J. Chem. Phys.* 107:1232–41
125. Souda R. 2006. Time-of-flight secondary ion mass spectroscopy analysis of Na adatoms interacting with water–ice film. *J. Chem. Phys.* 125:044706
126. Souda R. 2006. Evidence of deeply supercooled liquid water in interaction with LiCl. *J. Phys. Chem. B* 110:14787–91
127. Souda R. 2007. Two liquid phases of water in the deeply supercooled region and their roles in crystallization and formation of LiCl solution. *J. Phys. Chem. B* 111:5628–34
128. Souda R. 2007. Hydration of NaCl on glassy, supercooled-liquid, and crystalline water. *J. Phys. Chem. B* 111:11209–13
129. Mishima O, Stanley HE. 1998. The relationship between liquid, supercooled and glassy water. *Nature* 396:329–35
130. Souda R. 2006. Liquid-liquid transition in supercooled water investigated by interaction with LiCl and Xe. *J. Chem. Phys.* 125:181103
131. Souda R. 2008. Roles of deeply supercooled ethanol in crystallization and solvation of LiI. *J. Phys. Chem. B* 112:2649–54
132. Souda R. 2010. Roles of individual and cooperative motions of molecules in glass–liquid transition and crystallization of toluene. *J. Phys. Chem. B* 114:10734–39
133. Kawana S, Jones RAL. 2001. Character of the glass transition in thin supported polymer films. *Phys. Rev. E* 63:021501
134. Souda R. 2012. Nanoconfinement effects on the glass–liquid transition of vapor-deposited 1-pentene. *J. Phys. Chem. C* 116:7735–40
135. Souda R. 2006. Substrate and surfactant effects on the glass-liquid transition of thin water films. *J. Phys. Chem. B* 110:17524–30
136. LaPack MA, Pachuta SJ, Busch KL, Cooks RG. 1983. Surface modification by soft landing of reagent beams. *Int. J. Mass Spectrom. Ion Phys.* 53:323–26
137. Shen J, Yim YH, Feng B, Grill V, Evans C, Cooks RG. 1999. Soft landing of ions onto self-assembled hydrocarbon and fluorocarbon monolayer surfaces. *Int. J. Mass Spectrom.* 182/183:423–35
138. Denault JW, Evans C, Koch KJ, Cooks RG. 2000. Surface modification using a commercial triple quadrupole mass spectrometer. *Anal. Chem.* 72:5798–803
139. Judai K, Sera K, Amatsutsumi Si, Yagi K, Yasuike T, et al. 2001. A soft-landing experiment on organometallic cluster ions: infrared spectroscopy of  $\text{V}(\text{benzene})_2$  in Ar matrix. *Chem. Phys. Lett.* 334:277–84
140. Peng W-P, Goodwin MP, Chen H, Cooks RG, Wilker J. 2008. Thermal formation of mixed-metal inorganic complexes at atmospheric pressure. *Rapid Commun. Mass Spectrom.* 22:3540–48
141. Nagaoka S, Matsumoto T, Okada E, Mitsui M, Nakajima A. 2006. Room-temperature isolation of  $\text{V}(\text{benzene})_2$  sandwich clusters via soft-landing into *n*-alkanethiol self-assembled monolayers. *J. Phys. Chem. B* 110:16008–17

142. Matsumoto T, Nagaoka S, Ikemoto K, Mitsui M, Ara M, et al. 2009. Characterization of alkyl monolayer covalently bonded to Si(111) and soft-landing of vanadium-benzene sandwich clusters onto the alkyl monolayer substrate. *Eur. Phys. J. D* 52:99–102
143. Nagaoka S, Matsumoto T, Ikemoto K, Mitsui M, Nakajima A. 2007. Soft-landing isolation of multi-decker  $V_2(\text{benzene})_3$  complexes in an organic monolayer matrix: an infrared spectroscopy and thermal desorption study. *J. Am. Chem. Soc.* 129:1528–29
144. Nagaoka S, Ikemoto K, Matsumoto T, Mitsui M, Nakajima A. 2008. Thermal and hyperthermal collision-energy depositions of transition metal-benzene sandwich complexes onto a self-assembled *n*-octadecanethiol monolayer. *J. Phys. Chem. C* 112:6891–99
145. Peng W-P, Johnson GE, Fortmeyer IC, Wang P, Hadjar O, et al. 2011. Redox chemistry in thin layers of organometallic complexes prepared using ion soft landing. *Phys. Chem. Chem. Phys.* 13:267–75



# Contents

Is the Focus on “Molecules” Obsolete? <i>George M. Whitesides</i> .....	1
Synthetic Nanoelectronic Probes for Biological Cells and Tissues <i>Bozhi Tian and Charles M. Lieber</i> .....	31
Multiplexed Sensing and Imaging with Colloidal Nano- and Microparticles <i>Susana Carregal-Romero, Encarnación Caballero-Díaz, Lule Beqa, Abuelmagd M. Abdelmonem, Markus Ochs, Dominik Hübner, Bartolome Simonet Suau, Miguel Valcarcel, and Wolfgang J. Parak</i> .....	53
Nanobiodevices for Biomolecule Analysis and Imaging <i>Takao Yasui, Noritada Kaji, and Yoshinobu Baba</i> .....	83
Probing Molecular Solids with Low-Energy Ions <i>Soumabha Bag, Radha Gobinda Bhui, Ganapati Natarajan, and T. Pradeep</i> .....	97
Microfluidic Chips for Immunoassays <i>Kwi Nam Han, Cheng Ai Li, and Gi Hun Seong</i> .....	119
Semiconductor Quantum Dots for Bioimaging and Biodiagnostic Applications <i>Brad A. Kairdolf, Andrew M. Smith, Todd H. Stokes, May D. Wang, Andrew N. Young, and Shuming Nie</i> .....	143
Environmental Mass Spectrometry <i>Albert T. Lebedev</i> .....	163
Evidence-Based Point-of-Care Diagnostics: Current Status and Emerging Technologies <i>Cangel Pui Yee Chan, Wing Cheung Mak, Kwan Yee Cheung, King Keung Sin, Cheuk Man Yu, Timothy H. Rainer, and Reinhard Renneberg</i> .....	191
Adsorption and Assembly of Ions and Organic Molecules at Electrochemical Interfaces: Nanoscale Aspects <i>Soichiro Yoshimoto and Kingo Itaya</i> .....	213

Structural Glycomic Analyses at High Sensitivity: A Decade of Progress <i>William R. Alley, Jr. and Milos V. Novotny</i> .....	237
Structures of Biomolecular Ions in the Gas Phase Probed by Infrared Light Sources <i>Corey N. Stedwell, Johan F. Galindo, Adrian E. Roitberg, and Nicolas C. Polfer</i> .....	267
Next-Generation Sequencing Platforms <i>Elaine R. Mardis</i> .....	287
Structure Determination of Membrane Proteins by Nuclear Magnetic Resonance Spectroscopy <i>Stanley J. Opella</i> .....	305
Scanning Electrochemical Cell Microscopy: A Versatile Technique for Nanoscale Electrochemistry and Functional Imaging <i>Neil Ebejer, Aleix G. Güell, Stanley C.S. Lai, Kim McKelvey, Michael E. Snowden, and Patrick R. Unwin</i> .....	329
Continuous Separation Principles Using External Microaction Forces <i>Hitoshi Watarai</i> .....	353
Modern Raman Imaging: Vibrational Spectroscopy on the Micrometer and Nanometer Scales <i>Lothar Opilik, Thomas Schmid, and Renato Zenobi</i> .....	379
The Use of Synchrotron Radiation for the Characterization of Artists' Pigments and Paintings <i>Koen Janssens, Matthias Alfeld, Geert Van der Snickt, Wout De Nolf, Frederik Vanmeert, Marie Radepont, Letizia Monico, Joris Dik, Marine Cotte, Gerald Falkenberg, Costanza Miliani, and Brunetto G. Brunetti</i> .....	399
Real-Time Clinical Monitoring of Biomolecules <i>Michelle L. Rogers and Martyn G. Boutelle</i> .....	427

## Indexes

Cumulative Index of Contributing Authors, Volumes 1–6 .....	455
Cumulative Index of Article Titles, Volumes 1–6 .....	459

## Errata

An online log of corrections to *Annual Review of Analytical Chemistry* articles may be found at <http://arjournals.annualreviews.org/errata/anchem>